

# Anisotropy of Magnetohydrodynamic Turbulence and the Polarized Spectra of OH Masers

William D. Watson<sup>1</sup>, Dmitri S. Wiebe<sup>1,2</sup>, Jonathan C. McKinney<sup>1</sup>, and Charles F. Gammie<sup>1,3</sup>

*University of Illinois, 1110 West Green Street, Urbana, IL 61801*

## ABSTRACT

We consider astrophysical maser radiation that is created in the presence of mildly supersonic, magnetohydrodynamic (MHD) turbulence. The focus is on the OH masers for which the magnetic field is strong enough that the separations of the Zeeman components are greater than the spectral linebreadths. A longstanding puzzle has been the absence of the Zeeman  $\pi$  components and the high circular polarization in the observed spectra of these masers. We first argue that the elongation of eddies along the field that has recently been recognized in MHD turbulence will enhance the optical depth parallel to the magnetic field in comparison with that perpendicular to the magnetic field. We then simulate maser emission with a numerical model of MHD turbulence to demonstrate quantitatively how the intensities of the linearly polarized  $\pi$  components are suppressed and the intensities of the nearly circularly polarized  $\sigma$  components are enhanced. This effect is also generic in the sense that most spectral lines in MHD turbulence with Mach number  $M \sim 1$  should have larger optical depth parallel to the magnetic field than perpendicular. The effect is reduced considerably when  $M < 1$ . The simulations also demonstrate that the velocity and magnetic field variations due to the turbulence can (but do not necessarily) cause one of the  $\sigma$  components to be much more intense than the other, as is often observed for mainline OH masers.

*Subject headings:* masers: OH—polarization—magnetic fields—MHD—turbulence

---

<sup>1</sup>Department of Physics.

<sup>2</sup>Permanent address: Institute of Astronomy of the RAS, 48, Pyatnitskaya str., 109017 Moscow, Russia.

<sup>3</sup>Department of Astronomy.

## 1. Introduction

Magnetohydrodynamic (MHD) turbulence is highly anisotropic (Goldreich & Sridhar 1995, hereafter GS; see also Montgomery & Turner 1981; Higdon 1984; for numerical confirmation see Cho & Vishniac 2000 and Maron & Goldreich 2001). According to the GS theory, turbulent eddies are elongated parallel to field lines, and this anisotropy increases as one progresses to smaller and smaller scales. In traversing a turbulent MHD gas, spectral line radiation will then typically sample regions that are extended parallel to the field. That is, the optical depth for spectral lines in MHD turbulence will be larger parallel to the field than perpendicular to the field. The GS theory predicts anisotropic scattering of radio waves, consistent with observations (e.g. Narayan, Anantharamaiah, & Cornwell 1989). It also predicts an angle-averaged spectrum that is consistent with measurements of radio wave fluctuations in the local interstellar medium (Armstrong, Rickett, & Spangler 1995).

Radiative transitions of atoms and molecules in the presence of a magnetic field are split into  $\sigma$  and  $\pi$  components according to the change in the quantum number for angular momentum along the magnetic field  $\Delta m = \pm 1$  or  $\Delta m = 0$ , respectively. The absorption and emission of radiation in these transitions by an isolated atom or molecule depends upon the angle  $\theta$  between the magnetic field and the direction of propagation of the radiation, and is proportional to  $(1 + \cos^2 \theta)$  for  $\sigma$  transitions and to  $2 \sin^2 \theta$  for  $\pi$  transitions (e.g., Condon & Shortley 1970, pg. 99). Radiation emitted in  $\sigma$  transitions is elliptically polarized—ranging from entirely circular at  $\theta = 0$  to entirely linear at  $\theta = 90^\circ$ , whereas that due to  $\pi$  transitions is 100% linearly polarized at all angles. Hence, if the magnitudes of the optical depths in directions close to that of the magnetic field are larger than in other directions, the  $\sigma$  components and the circularly polarized radiation will tend to be enhanced in comparison with the  $\pi$  components and the linearly polarized radiation. For masers, the effect of such differences can be exponentially amplified.

Among interstellar spectral lines, only the OH masers have Zeeman splittings that are greater than the spectral line breadths and they do, in fact, exhibit the characteristics described above. The OH masers at 1665 and 1667 MHz (“mainline” masers) occur widely in regions of star formation and have been especially well studied (e.g., Garcia-Barreto et al. 1988; Argon, Reid, & Menten 2000). Except possibly for a recent observation (Hutawarakorn, Cohen, & Brebner 2002), the  $\pi$  components have never been detected in this maser radiation. Circular polarization dominates and in some regions the radiation is essentially 100% circularly polarized. Nevertheless, a small fraction of the radiation often is linearly polarized. These spectral characteristics have remained a puzzle (e.g., Reid 2002) since the initial discoveries of masers in astronomy. Though the Zeeman splitting ordinarily is much smaller for other masing transitions of OH, the  $\pi$  components seem to be absent and circular

polarization also seems to dominate for these (Baudry & Diamond 1998 [13 GHz]; see also Baudry et al. 1997 [6 GHz]). Gray and Field (1995) have emphasized that the  $\sigma$  and  $\pi$  radiation of the OH masers will tend to be beamed parallel and perpendicular, respectively, to the magnetic field.

A secondary polarization characteristic of the OH masers is that, commonly, only one of the two  $\sigma$  components of the 1665/1667 MHz transitions is detected from a particular maser location in observations that are performed at the highest possible angular resolution, though comparable numbers of masers with single right or single left circular polarization may be observed from the entire cluster of masers. For other masing transitions of OH, both  $\sigma$  components more often are detected at the same location (e.g., Moran et al. 1978; Caswell & Vaile 1995). The tendency for one of the  $\sigma$  components of the 1665/1667 MHz transitions to be much stronger than the other has often been attributed to shifts in the resonant frequency caused by gradients in the Doppler velocity and in the magnetic field that partially cancel for one of the  $\sigma$  components, but not for the other (Cook 1966). Actually, a velocity gradient alone is sufficient to create a single, sharp spectral line with a single sense of circular polarization if the change in velocity through the maser is as large as the Zeeman splitting and the maser is at least partially saturated (Deguchi & Watson 1986; Nedoluha & Watson 1990). In either case, the observation that single components with both senses of circular polarization occur in close proximity is more suggestive of the randomness associated with turbulence than to large scale gradients, which would tend to produce only one sense of the circular polarization for masers that are located close to one another.

The calculations of this Paper explore in more detail how well the anisotropy of the medium caused by MHD turbulence can serve as the basis for an understanding of the polarization characteristics of the OH masers, and conversely, whether these observed characteristics may be evidence of the nature of MHD turbulence in the interstellar gas. Standard methods are employed for computing a number of simulations of turbulent, compressible MHD to serve as representative “cubes” of velocities, magnetic fields and densities of the masing medium. These cubes are used to represent the regions of interstellar clouds in which clusters of OH masers are found. The coupled radiative transfer equations for the Stokes intensities are then solved as a function of Doppler velocity by numerical integration for a large number of uniformly spaced rays of maser radiation that pass through the cube at various angles. A comparison of the optical depths computed without the effect of maser saturation for the rays parallel and perpendicular to the direction of the average magnetic field provides a robust indication that the anisotropy of MHD turbulence has a significant effect. In examining the computed spectra, we focus on the brightest rays. These cover only a small fraction of the entire surface, just as the observed masers cover only a small fraction of the surface of the cloud in which they occur. We begin with general considerations for

both the MHD turbulence and the maser polarization (§2) before giving a more detailed description of the basic equations for the calculations (§3). The results of the computations are presented in §4. In §5, we discuss further the requirements for the MHD anisotropies to be applicable in the environments of the OH masers. We also reason in §5 that Faraday rotation, which has been mentioned as a possible cause for the absence of the  $\pi$  components of OH masers, is an unlikely explanation.

## 2. General Considerations

### 2.1. MHD Turbulence

The statistical properties of MHD turbulence can be partially characterized by the structure function

$$v_{i,\boldsymbol{\lambda}}^2 = \langle (v_i(\mathbf{r}) - v_i(\mathbf{r} + \boldsymbol{\lambda}))^2 \rangle. \quad (1)$$

We will use the shorthand  $v_{\parallel}$  to indicate the structure function for the velocity component parallel to the magnetic field, and  $v_{\perp}$  to indicate the structure function for either of the two perpendicular components. The quantity  $v_{\lambda}^2$  means  $(v_{\parallel}^2 + 2v_{\perp}^2)$  averaged over all directions for the separation vector  $\boldsymbol{\lambda}$ . For Kolmogorov-like turbulence,  $v_{\lambda} \sim v_L(\lambda/L)^{1/3}$ , where  $v_L$  is the three dimensional velocity dispersion on the outer scale  $L$ .

At any scale  $\lambda$  it is useful to consider two characteristic dimensionless parameters: the sonic Mach number  $M_{\lambda} \equiv v_{\lambda}/c_s$  and the Alfvén Mach number  $M_{A,\lambda} \equiv v_{\lambda}/v_A$  (we will assume that  $\rho$  and  $v_A$  do not scale with  $\lambda$ ). When  $M_L \equiv M \ll 1$  turbulence is approximately incompressible; when  $M_A \ll 1$  it is strongly constrained by the presence of the mean magnetic field, which it cannot bend. Because  $v_{\lambda}$  is typically an increasing function of  $\lambda$ ,  $M_{\lambda}$  and  $M_{A,\lambda}$  are both small at small  $\lambda$ . MHD turbulence is therefore incompressible and mean field dominated on small scales. This was the case considered by GS in their theory of strong MHD turbulence.

The OH maser lines, however, will be little influenced by turbulence unless the Doppler shift associated with bulk motion of the gas is at least comparable to the thermal linewidth of OH. This requires  $M_L \gtrsim 1$ , which implies that the turbulence is compressible. There is currently no good theory for compressible MHD turbulence. Simulations (Cho & Lazarian 2003; Vestuto, Ostriker, & Stone 2003) indicate, however, that the scalings introduced by GS may be valid up to  $M_L \sim$  a few. Encouraged by this, we will employ GS’s scalings in the estimates that follow.

We want to estimate the line-center optical depth  $\tau_0$  in an unsaturated maser line. For

simplicity we will make an estimate assuming that the optical depth at Doppler velocity  $v$  has the form

$$\tau_v \simeq \frac{\sigma}{v_{th}} \int ds e^{-(v-v_{turb}(s))^2/v_{th}^2} \quad (2)$$

where  $\sigma$  is a constant,  $v_{turb}(s)$  is the component of the turbulent velocity along the line of sight,  $v_{th}$  is the thermal velocity of OH, and the integral is taken along the line of sight. Most of the optical depth will come from a region of size  $l_{th}$  where  $v_{turb}(s)$  changes by of order  $v_{th}$ . If  $l_{th}$  is smaller than the size of the masing cloud (i.e.,  $v_L > v_{th}$ ), then  $\tau_0 \sim (\sigma/v_{th})l_{th}$ . Otherwise we simply have  $\tau_0 \sim (\sigma/v_{th})L$ . We will assume that we can estimate  $l_{th}$  using the structure function (1). Thus to find the line center optical depth we need to find  $l_{th}$  such that  $v_{l_{th}} \sim v_{th}$ .

Perpendicular to the mean magnetic field, the GS theory gives

$$v_{\perp}(\lambda_{\perp}) \approx \frac{v_L}{\sqrt{3}} \left( \frac{\lambda_{\perp}}{L} \right)^{1/3}, \quad (3)$$

as in the Kolmogorov theory. Then

$$l_{th,\perp} = L \left( \frac{\sqrt{3} v_{th}}{v_L} \right)^3, \quad (4)$$

where we have normalized the perpendicular velocities by assuming isotropy at the outer scale:

$$v_{\parallel,L}^2 = v_{\perp,L}^2 = \frac{v_L^2}{3}. \quad (5)$$

A more general treatment is possible, but this simplified analysis will serve to make our point.

To find  $l_{th,\parallel}$  we must invoke a weak extension of the GS theory, because GS theory considers incompressible Alfvénic fluctuations which are necessarily perpendicular to the mean field. But models of weakly compressible turbulence (Lithwick & Goldreich 2001), numerical models of compressible turbulence (Cho & Lazarian 2003; Vestuto, Ostriker, & Stone 2003), and of the cascade of slow (pseudo-Alfvén) waves in incompressible turbulence (Cho, Lazarian, & Vishniac 2002) suggest that  $v_{\parallel}$  should have the same spectrum as  $v_{\perp}$ .

Correlations along the field can be determined from GS's relation  $\lambda_{\parallel} \sim \lambda_{\perp}^{2/3}$ , which defines a surface of constant correlation amplitude. Then

$$v_{\parallel}(\lambda_{\parallel}) \approx \frac{v_L}{\sqrt{3}} \left( \frac{\lambda_{\parallel}}{L} \right)^{1/2}, \quad (6)$$

and

$$l_{th,\parallel} = L \left( \frac{\sqrt{3}v_{th}}{v_L} \right)^2. \quad (7)$$

Again, we have assumed isotropy at the outer scale.

Then the ratio of parallel to perpendicular optical depths is

$$\frac{l_{th,\parallel}}{l_{th,\perp}} = \frac{v_L}{\sqrt{3}v_{th}}, \quad (8)$$

provided that  $v_L > v_{th}\sqrt{3}$  (if the turbulence is subthermal throughout the emitting region then the parallel and perpendicular optical depths differ only slightly). Parallel optical depths should therefore typically be larger than perpendicular optical depths for mildly supersonic turbulence.

When will this effect be absent? The parallel optical depth can exceed the perpendicular optical depths only if  $v_L/v_{th} \gtrsim \sqrt{3}$ . Notice that  $v_L/v_{th} = M_L\sqrt{m_{\text{OH}}/2\mu} \approx 2.1M_L$ , where  $\mu$  is the mean molecular weight of the gas and  $m_{\text{OH}}$  is the mass of the OH molecule, so only  $M_L \sim 1$  is required for an interesting ratio of optical depths parallel and perpendicular to the field, and conversely the effect should vanish for subsonic turbulence.

The key is, of course, the anisotropy of the turbulence. We expect that MHD turbulence is nearly isotropic unless  $M_{A,l_{th}} \lesssim 1$ . That is, the field needs to be strong enough to place a dynamical constraint on the masing eddies. Since

$$M_{A,l_{th}} = \frac{v_{l_{th}}}{v_A} = \frac{v_{th}}{v_A} \sim \beta^{1/2}, \quad (9)$$

the effect is absent unless  $\beta \lesssim 1$ .

The estimates in this section suggest that the optical depth to OH maser lines should be larger parallel to the mean magnetic field than perpendicular to it, provided that the turbulence is mildly supersonic and  $\beta \lesssim 1$ . Our estimates are encouraging but not conclusive because they rely on an extension of the GS theory. In addition, strong maser spots are rare events whose frequency may not be well described by the two-point statistics considered here. A test of these estimates against a simulation of compressible 3D MHD turbulence is required.

## 2.2. Polarized Maser Radiation

The transfer equations for polarized radiation (see §3) can readily be solved for a uniform medium in the regime where the maser is unsaturated and the Zeeman splitting of the

components is much greater than the spectral linebreadth so that overlap can be ignored (Goldreich, Keeley, & Kwan 1973, hereafter GKK, pg. 124). For an optical depth of magnitude  $\tau_0$ , the intensities  $I_{\pm}$  of the two  $\sigma$  components and  $I_0$  of the  $\pi$  component are given by

$$I_{\pm} \simeq (I_c/2) \exp[\tau_0(1 + \cos^2 \theta)/2] \quad (10)$$

and

$$I_0 \simeq (I_c/2) \exp[\tau_0 \sin^2 \theta] \quad (11)$$

for propagation at an angle  $\theta$  from the magnetic field when the amplification is large as is the case for astrophysical masers. Here,  $I_c$  is the unpolarized continuum radiation that is incident on the far side of the maser and serves as the “seed” radiation. In terms of the Stokes parameters  $V$  and  $Q$  that measure the circular and linear polarization, respectively, the fractional polarizations are

$$\frac{V_{\pm}}{I_{\pm}} = \frac{\pm 2 \cos \theta}{1 + \cos^2 \theta}, \quad (12)$$

$$\frac{Q_{\pm}}{I_{\pm}} = \frac{\sin^2 \theta}{1 + \cos^2 \theta}, \quad (13)$$

$$\frac{V_0}{I_0} = 0, \quad (14)$$

and

$$\frac{Q_0}{I_0} = -1, \quad (15)$$

where the direction of the linear polarization is parallel (perpendicular) to the direction of the magnetic field projected on the sky when  $Q$  is negative (positive). A reasonable estimate for the mainline OH masers is  $\tau_0 \simeq 20$ . From equations (10) and (11), the intensity  $I_{\pm}$  of the  $\sigma$  components can then be seen to peak strongly at small angles  $\theta$  where circular polarization dominates. The intensity  $I_0$  of the linearly polarized  $\pi$  components is similarly peaked in directions that are perpendicular to the magnetic field. We would not then expect to observe the  $\sigma$  and  $\pi$  components together from the same region if the magnetic field there is uniform and the masers are unsaturated. However, statistically we are equally likely to observe regions where the magnetic field makes large angles with the line-of-sight and regions where it makes small angles. Hence, in conflict with the observations, comparable numbers of  $\sigma$  and  $\pi$  components would be detected when a number of independent regions are observed. The situation is even worse for understanding the absence of  $\pi$  components in the limit of highly saturated masing. All three intensities ( $I_{\pm}$  and  $I_0$ ) become equal and independent of angle  $\theta$  with fractional polarizations that are the same as given by equations (12)-(15) for unsaturated masers (GKK, pg. 122).

On the other hand, if the medium is anisotropic and the optical depth for unsaturated masing is greater in directions close to the magnetic field than perpendicular to the field lines, then  $I_{\pm}$  near  $\theta = 0$  can be much greater than  $I_0$  near  $\theta = 90^\circ$  (or at any other angle) even for modest fractional differences in the optical depths according to equations (10) and (11). It is then possible that the  $\sigma$  components near  $\theta = 0$  are strong enough to be detected while the  $\pi$  components near  $\theta = 90^\circ$  or at any other angle are too weak to be detected. As described above, the anisotropy of MHD turbulence can cause the optical depths along the field lines to be greater than those perpendicular to the field lines.

Trapped infrared radiation and perhaps other processes can randomize the thermal velocities and the populations of the magnetic substates of the masing molecules at a rate  $\gamma$ . This rate can be greater than the rate  $\Gamma$  at which an excited masing state decays as a result of all processes other than the stimulated emission by the maser radiation which proceeds at a rate  $R$  (Goldreich, Keeley, & Kwan 1973; Anderson & Watson 1993). For simplicity, we take the rate  $\gamma$  to be the same for randomizing both the velocities and substate populations. A regime  $\gamma > R > \Gamma$  then exists in which the maser is saturated in the sense that the maser radiation influences the molecular populations and the amplification is approximately linear (as opposed to exponential) with the length of the maser in a uniform medium, but still behaves like an unsaturated maser in retaining angular distributions for  $\sigma$  and  $\pi$  components of the form given by equations (10) and (11). The spectral line narrowing of unsaturated maser amplification to produce subthermal linebreadths also is preserved in this regime. Just as for completely unsaturated masers, the velocity distribution of the masing molecules is Maxwellian and the populations of an energy level are equal in this regime.

### 3. Basic Methods

#### 3.1. Numerical Model

Our analysis is based on a numerical model of decaying MHD turbulence. In the model, we integrate the equations of compressible, ideal MHD:

$$\frac{\partial \rho}{\partial t} + \nabla \cdot (\rho \mathbf{v}) = 0, \quad (16)$$

$$\frac{\partial v}{\partial t} + (\mathbf{v} \cdot \nabla) \mathbf{v} = -\frac{\nabla p}{\rho} + \frac{(\mathbf{B} \cdot \nabla) \mathbf{B}}{4\pi\rho} - \frac{\nabla B^2}{8\pi\rho}, \quad (17)$$

$$\frac{\partial \mathbf{B}}{\partial t} = \nabla \times (\mathbf{v} \times \mathbf{B}), \quad (18)$$



and as usual  $\rho \equiv$  density,  $\mathbf{v} \equiv$  velocity,  $p \equiv$  pressure, and  $\mathbf{B} \equiv$  magnetic field. We use an isothermal equation of state  $p = c_s^2 \rho$ , with  $c_s = \text{constant}$ . This equation of state is valid in regions where the cooling time is much shorter than a dynamical time. No forcing term is employed, and the model is nonself-gravitating. The scheme contains no explicit resistivity or viscosity, although a nonlinear artificial viscosity is used to capture shocks.

The basic equations are integrated in a cubic, periodic domain of linear size  $L$ . The initial state consists of a uniform medium,  $\rho = \rho_0 = \text{constant}$ ,  $\mathbf{B} = B_{x0} \hat{\mathbf{x}}$ , with a superposed velocity perturbation  $\delta \mathbf{v}$ . The  $\delta \mathbf{v}$  is a Gaussian, random field with the following properties: (1) the spectrum  $\langle \delta \mathbf{v}_{\mathbf{k}}^2 \rangle \sim k^{-11/3}$  for  $k_{max} > k > k_{min}$  (this is a Kolmogorov spectrum); (2)  $k_{max} = 32(2\pi/L)$ ; (3)  $k_{min} = 2(2\pi/L)$ , (4)  $\nabla \cdot \delta \mathbf{v} = 0$ ; (5) the modes with  $k = k_{min}$  had their amplitudes set equal to the expectation value.

The power-law spectrum was adopted to hasten the relaxation of the turbulent state. A Kolmogorov slope was chosen (rather than the  $-4$  expected of strongly compressible turbulence) because our models have a Mach number of a few and are therefore only weakly compressible. Experience suggests that the evolution is insensitive to the precise choice of index as long as most of the power is concentrated in the long wavelength spatial modes.

A fixed (rather than resolution-dependent)  $k_{max}$  was introduced to permit evolutions of identical realizations of the power spectrum at different resolutions. The  $k_{min}$  was set at a wavenumber corresponding to a wavelength  $L/2$  rather than  $L$  in order to increase the number of modes that contribute significantly to the power. This reduced run-to-run variations in the evolution, and was also the motivation for fixing the amplitude of modes with  $k = k_{min}$ . The initial velocity field was made incompressible to facilitate comparison with earlier runs (e.g. Stone, Ostriker, & Gammie 1998) which used a similar constraint in order to minimize turbulent dissipation.

The initial conditions are scaled so that  $L = c_s = \rho_0 = 1$ . These quantities can then be rescaled to match physical conditions in a masing region.

Our numerical method is based on the ZEUS scheme (Stone & Norman 1992). ZEUS is an operator-split, finite difference scheme on a staggered mesh. Constrained transport (Evans & Hawley 1988) is used to guarantee that  $\nabla \cdot \mathbf{B} = 0$  to machine precision. Our version of the ZEUS code was parallelized by one of us (JCM) and run on NCSA's Platinum cluster.

Our numerical models have 3 parameters: the rms Mach number of the initial conditions, the mean magnetic field strength (which can be parameterized in terms of the initial  $\beta^{-1} \equiv v_A^2/c_s^2 = B_{x0}^2/(4\pi\rho_0 c_s^2)$ ), and the numerical resolution. We have studied runs at resolution  $66^3, 128^3$  (our default resolution) and  $256^3$ . Our results are insensitive to resolution. The

initial rms Mach number in all of our computations is four. Three values for the initial  $v_A/c_s$  are considered—1, 3, and 10. For each of these  $v_A/c_s$ , the MHD equations are integrated for three independent choices for the ensemble of random numbers that specifies the initial amplitudes of the various Fourier components  $\delta\mathbf{v}_{\mathbf{k}}$ . We thus obtain three sequences in time of MHD cubes to represent the interstellar gas for each  $v_A/c_s$ .

### 3.2. Maser Radiative Transfer for the Stokes Parameters

The maser radiation is calculated with the simplification that each ray is treated as an independent linear maser—a standard simplification for astrophysical masers. Since the focus in calculating the intensities is on only the small fraction of the rays through the computational cube that are the brightest and represent the observed maser features, the assumption that they can be treated as independent is reasonable since it is less likely that they will intersect the paths of other strong rays that are propagating in different directions. In any case, interaction between the rays can only have an effect when the maser is saturated and the effect would be to strengthen the stronger maser beam at the expense of the weaker. Since the  $\sigma$  radiation tends to be the stronger in the scenario here, the effect would be to further enhance the  $\sigma$  radiation relative to the  $\pi$  radiation, and hence to strengthen the conclusions of this investigation that MHD anisotropy tends to suppress the  $\pi$  component. In addition, the present calculations are limited to masing under conditions of modest saturation.

The calculations are performed for an angular momentum  $J = 1 \rightarrow 0$  transition and, as is commonly done, the results are assumed to be indicative for molecular states with higher angular momenta. For the OH masers, it is clear that the Zeeman frequency (sometimes “ $g\Omega$ ”) is much larger than the rates for stimulated emission and other competing processes. In this regime, the radiative transfer equations for the Stokes parameters  $I, Q, U,$  and  $V$  are of the same form as for ordinary spectral line radiation and for the purposes here can be expressed as

$$\frac{d}{ds} \begin{pmatrix} I \\ Q \\ U \\ V \end{pmatrix} = \begin{pmatrix} A & B & 0 & C \\ B & A & 0 & 0 \\ 0 & 0 & A & 0 \\ C & 0 & 0 & A \end{pmatrix} \times \begin{pmatrix} I \\ Q \\ U \\ V \end{pmatrix} \quad (19)$$

from Watson & Wyld (2001) (which rephrases GKK for the relevant regime) where

$$A = (1 + \cos^2 \theta)n(f_+ + f_-) + 2nf_0 \sin^2 \theta, \quad (20)$$

$$B = \sin^2 \theta(f_+ + f_- - 2f_0)n, \quad (21)$$

and

$$C = 2n \cos \theta (f_+ - f_-). \quad (22)$$

Here, the  $f$ 's are the Maxwellian distributions for the component of the molecular velocity along the line-of-sight and  $n$  is the difference between the normalized populations of the magnetic substates of the upper  $J = 1$  energy level and the normalized population of the  $J = 0$  lower energy level. The  $f_{\pm}$  and  $f_0$  are evaluated at the velocities  $v_{\pm}$  and  $v_0$  obtained from  $(1 - v_{\pm}/c)\omega = \omega_R \pm g\Omega/2$  and  $(1 - v_0/c)\omega = \omega_R$  where  $\omega$  is the angular frequency of the intensities in equation (13),  $\omega_R$  is the resonance frequency of the masing transition for a molecule at rest and  $\pm g\Omega/2$  are the splittings of the  $m = \pm 1$  substates due to the Zeeman effect. Only a single population difference enters in equations (20)–(22) because the calculations will be restricted to the regime of saturation ( $\gamma > R$ ) where the populations of the magnetic substates of an energy level are equal due to the assumed rapid cross/velocity relaxation. The population differences  $n$  are found by solving the rate equations in this regime using the standard idealization of “phenomenological” pump  $\Lambda$  and loss  $\Gamma$  rates

$$n = \frac{\Delta\Lambda/\Gamma}{1 + 4(R_+ + R_- + R_0)/3\Gamma} \quad (23)$$

Here  $R_+$ ,  $R_-$ , and  $R_0$  are the rates for stimulated emission for the  $m = \pm 1$  and 0 substates (see Watson & Wyld 2001 for detailed expressions for  $R_+$ ,  $R_-$ , and  $R_0$ ), and  $\Delta\Lambda$  is the difference between the pump rates per substate into the upper and lower energy levels. Also, note that in the above definitions  $\Delta\Lambda$  does not involve the Maxwellian velocity distributions which are included as the  $f$ 's. As a further simplification, only the values of  $R_+$ ,  $R_-$ , and  $R_0$  at the line centers of the  $\sigma$  and  $\pi$  components in the local rest frames moving with the turbulent velocities are used in equation (23). The completely accurate procedure would involve averaging over the absorption profile. The inaccuracy introduced by this simplification is negligible for this investigation since the emergent intensities near line center are adequate for the purposes here, and since the degree of saturation will be modest (and we have confirmed that the differences between the results with and without saturation are small).

External continuum radiation is assumed to provide the seed radiation for the maser in equation (19). Whether external continuum or spontaneous emission provides the seed radiation is unimportant for the emergent radiation. The distance  $s$  is measured along the straight-line path of the ray and the Stokes intensities in equation (13) are expressed in dimensionless form. They are actual intensities divided by a characteristic “saturation intensity”  $I_s = 8\hbar\omega_R^3\Gamma/(3\pi c^2 A_E \Delta\Omega)$ , where  $A_E$  is the Einstein A-value for the transition and  $\Delta\Omega$  is the solid angle into which the maser radiation is beamed. When  $I = 1$  the rate for stimulated emission is approximately equal to the decay rate  $\Gamma$  for the molecular states.

The uncertain beaming angle of the maser radiation is thus incorporated into the definition of  $I_s$  as is customary for relating the intensity and the mean intensity “ $J$ ” for the linear maser (e.g., Watson & Wyld 2003).

Equation (19) is expressed in the coordinate system in which the axis of quantization for the magnetic substates is along the magnetic field. That is, the “z-axis” is along the magnetic field. Stokes  $Q$  and  $U$  also depend on the orientation of the coordinate system and hence upon the direction of  $\mathbf{B}$ . However, in a turbulent medium the direction of  $\mathbf{B}$  changes along the path of a ray of maser radiation. It is thus necessary to transform  $Q$  and  $U$  with a rotation of the coordinate system at each step of the integration along a ray to express  $Q$  and  $U$  in the coordinate system in which equation (13) is applicable. If the magnetic field rotates by an angle  $\phi$  when projected onto the plane perpendicular the direction of propagation,  $Q$  and  $U$  in the coordinate system after the rotation are related to the same quantities  $Q'$  and  $U'$ , but expressed in the system before the rotation, by  $Q = Q' \cos 2\phi + U' \sin 2\phi$  and  $U = -Q' \sin 2\phi + U' \cos 2\phi$  (e.g., Chandrasekhar 1960, pg. 34).

When turbulent velocities along the line-of-sight  $v_{turb}$  are incorporated explicitly and  $g\Omega$  is expressed in terms of the magnetic field and the magnetic moment  $\mu$ , the  $f$ 's become  $f_{\pm} = F \exp(-(v - v_{turb} \pm \mu B)^2/v_{th}^2)$  and  $f_0 = F \exp(-(v - v_{turb})^2/v_{th}^2)$ . In these,  $v$  and  $v_{th}$  are, respectively, the Doppler velocity at which the Stokes intensities in equation (19) are specified and the thermal velocity  $v_{th} = (2kT/m_{OH})^{1/2}$  of the OH molecules ( $F$  is the normalization constant for a Maxwellian).

To solve equation (19), it is necessary to specify (1) the radiation that is incident on the far side of the masing cube to serve as the seed radiation, (2) the Zeeman splitting (or more correctly  $\mu$ ), and (3) the pumping rate  $\Delta\Lambda$ .

The incident continuum radiation is assumed to be unpolarized so that the initial values for the Stokes intensities are  $Q = U = V = 0$  and  $I = I_c$ . For an assumed brightness temperature of 30 K for the external continuum seed radiation, decay rate  $\Gamma = 0.03 \text{ s}^{-1}$ , and a beaming angle  $\Delta\Omega = 5 \times 10^{-3}$  ster,  $I_c = 10^{-10}$  when expressed in units of  $I_s$ .

All of the computations in the Figures are obtained with this  $I_c$ , though we have verified that the results are insensitive to changes in  $I_c$  by a few powers of ten. For the Zeeman splitting, we adopt  $(\mu B_{avg}/v_{th}) = 9$  for the computations in the Figures. This corresponds to a separation of  $5.4 \text{ km s}^{-1}$  between the two  $\sigma$  components when the gas temperature is 100 K. We have also performed computations with  $(\mu B_{avg}/v_{th}) = 4.5$  and have verified that the essential behavior of the spectra is unchanged within this range of Zeeman splittings which is representative of what is observed for the OH masers with distinct Zeeman components. We choose to specify  $\mu B_{avg}/v_{th}$  instead of simply  $\mu$  so that in all of our computations, the

Zeeman components will be well separated as in the observations and the splitting will be essentially the same for purposes of comparison.

We consider two idealizations for  $\Delta\Lambda$ :  $\Delta\Lambda$  is equal to the density multiplied by a constant, and  $\Delta\Lambda$  is simply constant throughout the computational cube. All of the results that we present in the Figures are obtained with  $\Delta\Lambda$  proportional to density. The results are generally similar when  $\Delta\Lambda = \text{constant}$  is used, and we reason that the conclusions of our investigation are not sensitive to this idealized treatment of the pumping. The constant that multiplies the density for the pumping is chosen separately for each cube so that  $I = 1$  for the strongest ray of the  $128^2$  rays that emerge parallel to the magnetic field from the  $128^2$  grid points on the face of the particular cube. Representative computations also are performed when this pumping constant is chosen so that the strongest ray has  $I = 0.1$  and  $I = 10$ . The differences are not significant.

#### 4. Results

When the effects of saturation are ignored (i.e.,  $n$  is set to be  $\Delta\Lambda/\Gamma$  regardless of the intensity) in solving equation (13) for the intensities, an unsaturated optical depth  $\tau$  can be obtained for the intensity  $I$ ,

$$\tau = \ln(I/I_c) \tag{24}$$

Equation (13) is integrated along the paths of each of the  $128^2$  rays that emerge from the grid points on the faces of the computational cubes. The unsaturated optical depth  $\tau$  at the peak intensity is then obtained for each ray. Representative histograms of these optical depths are given in Figure 1 for rays that are parallel and perpendicular to the direction of the average magnetic field in the cubes (with the normalization that  $I = 1$  for the brightest ray in the parallel direction for each cube). The expected result that the parallel rays should have larger optical depths is evident for  $v_A/c_s \gtrsim 3$ . A similar trend with  $v_A/c_s$  is evident in all of the 81 cubes that were studied. The 81 cubes were obtained by considering the solutions at nine equally spaced times (separated by  $\Delta t = 0.2L/c_s$ ) for each of the nine sets of initial conditions for which the MHD equations are integrated. Although there is considerable overlap in the histograms for  $v_A/c_s = 3$ , the masing spots are represented by the brightest rays from the face of the cube and these are due to only a small number of the largest optical depths. There is no overlap even at  $v_A/c_s = 3$  for the tails of the distributions at large optical depth. It might be surprising that the perpendicular optical depths tend to be larger than the parallel optical depths in our calculations for  $v_A/c_s = 1$ . This result is somewhat artificial. It occurs because the turbulent velocities are smaller in the MHD computations for  $v_A/c_s = 1$  than for  $v_A/c_s = 3$  and  $v_A/c_s = 10$ , and they also are smaller

than the thermal velocity  $v_{th}$  of the OH. When  $v_{turb}$  is less than  $v_{th}$  in  $f_{\pm}$  and  $f_0$ , the effect of the MHD anisotropy of  $v_{turb}$  to enhance the parallel, relative to the perpendicular, rays is reduced or disappears. In contrast, the variation in  $(\mu B/v_{th})$  along a ray is still significant (at least for the adopted  $\mu B_{avg}/v_{th} = 9$ ) and reduces the optical depths for the  $\sigma$  components, but not for the  $\pi$  components since  $f_0$  does not depend on  $B$ . We have verified that the histograms for the parallel and perpendicular rays coincide for  $v_A/c_s = 1$  when the Zeeman splitting is set to zero, as would be expected.

A factor in the decrease in the anisotropy of the optical depths in Figure 1 with decreasing  $v_A/c_s$  must be the decrease in the turbulent velocities that results when the initial  $v_A/c_s$  is reduced while the initial rms turbulent velocities remain fixed in the MHD simulations. The rms values for the components of the turbulent velocities in a specific direction (i.e., parallel or perpendicular to the direction of the magnetic field) are approximately  $0.9c_s$ ,  $0.7c_s$  and  $0.4c_s$  for the turbulent cubes with initial  $v_A/c_s = 10, 3$ , and  $1$ , respectively, in Figures 1-4. However, this cannot be the only factor. In the turbulent cubes from the time evolution of the MHD equations that we use, the component rms velocities for  $v_A/c_s = 3$  decrease to approximately  $0.4c_s$  without a significant change in the anisotropy as indicated by histograms such as in Figure 1. A key difference emerges when we examine the dispersions (i.e., standard deviations) in velocity along the paths of individual rays. For the simulated turbulent cubes with  $v_A/c_s = 3$  and  $10$ , the average dispersion in the component of the velocity along the line of sight is much smaller for rays that propagate parallel to the magnetic field than for rays that propagate perpendicular to the magnetic field. The two dispersions are equal for turbulent cubes computed with  $v_A/c_s = 1$  (for all  $v_A/c_s$ , the rms of the components of the velocities and of the turbulent magnetic fields parallel and perpendicular to the magnetic field are equal). This indicates that the turbulent medium becomes significantly anisotropic when  $\beta = c_s^2/v_A^2$  is near  $0.1$ , at least in our calculations.

The coupled equations (19) are now integrated with the effects of saturation included with rapid cross/velocity relaxation as described in the foregoing Section (i.e.,  $n$  is given by equation 23) for turbulent cubes that are computed with  $v_A/c_s = 3$ . Computations are performed for a range of intermediate angles as well as for propagation parallel and perpendicular to the magnetic field. At each angle, the coupled equations are solved for the rays that emerge from the  $128^2$  grid points on the face of a cube. The peak intensity of the brightest ray at each angle is plotted in Figure 2 for representative results. To agree with the observations, all  $\pi$  components and rays with large fractional linear polarization must be too weak to be detected. Hence, the focus is on the brightest rays. Since there is considerable scatter in the intensities in Figure 2, we encompass the intensity points with a shaded band to provide a sense of the behavior of the angular variation. The main result in Figure 2 is that the intensities within approximately  $20^\circ$  of the direction of the average

magnetic field are greater by a factor of about 100 or more than those at angles near  $90^\circ$ . All of these more intense rays near  $0^\circ$  are  $\sigma$  components as indicated their high fractional circular polarization, as well as by their Doppler velocities which are quite close to  $\pm\mu B_{avg}$ . All of the weaker rays near  $90^\circ$  are 100 % linearly polarized and are  $\pi$  components (they are at essentially zero Doppler velocity). Note that, as discussed in §3, the pumping is chosen so that  $I = 1$  for the brightest ray that is parallel to the average magnetic field in each cube. When there is no turbulence (the cube is uniform) and the masing is treated in the unsaturated limit, the angular variations of the intensities for  $\sigma$  and  $\pi$  components are given by the simple functions of equations (10) and (11). For comparison, these functions also are plotted in Figure 2 with  $\tau_0$  chosen so that  $I = 1$  at  $0^\circ$ , as well ( it also follows in this case that  $I = 1$  at  $90^\circ$ ). Finally, not only is the polarization of the single brightest ray of a turbulent cube the same as that of a “pure”  $\sigma$  component at angles less than about  $20^\circ$  (essentially 100% circular), but the same is true for all of the rays at these angles that have intensities within 1% of the brightest rays. Likewise, the rays near  $90^\circ$  having intensities within 1% of the brightest rays at that angle are 100% linearly polarized (as expected for  $\pi$  components) and have the Doppler velocity expected for  $\pi$  components. Thus, only  $\sigma$  components within about  $20^\circ$  of the average magnetic field will be detected from the turbulent cube in Figure 2 when the observational sensitivity is 1% of the intensity of the brightest maser spot.

A grayscale map of the intensities that emerge from the surface of a representative cube with  $v_A/c_s = 3$  and parallel to the average magnetic field is shown in Figure 3. The general appearance seems compatible with that of observational maps. The spectra in the side panels of the three adjacent rays within a cluster demonstrates that a single feature of right circular polarization, a single feature of left circular polarization and a Zeeman pair can be in close proximity. The spectrum of the strongest feature in the entire map is a single feature that is 100% circularly polarized. All are at Doppler velocities expected for  $\sigma$  components ( $\pm\mu B_{avg}$ ).

Finally, a histogram is given in Figure 4 for the ratio of the peak intensities of the weaker to the stronger feature of a Zeeman pair for all rays with intensities greater than 3% of the most intense ray for the two turbulent cubes with  $v_A/c_s = 3$ , one of which is the cube used in Figure 1. The 3% is an estimate for the weakest features that will be recorded in the observations. One of the histograms in Figure 4 demonstrates that the description of the turbulence being used here is consistent with the observational result that only one of the two circularly polarized Zeeman components frequently is detected for the mainline 1665/1667 MHz masers. For the variations of the velocities and magnetic fields in other turbulent cubes (e.g., the other histogram in Figure 4), we find the full range of possibilities—in some the Zeeman pairs and unpaired components occur with comparable frequency, in others the Zeeman pairs are much more numerous and finally, there are many in which unpaired

components are completely absent. The rays in the histogram are subdivided according to peak intensity to explore whether the likelihood for an unpaired component depends on intensity. No such dependence stands out, though the Zeeman pairs are not among the most intense subgroup in this histogram.

The most intense rays from a cube depend on the tails of the distributions in Figure 1 at large optical depths. The tails of the distributions are, as is usually the case for tails of distributions, likely to be sensitive to details that are not well described in idealized models. However, the differences in the average optical depths in the distributions in Figure 1 provide compelling and robust evidence that the  $\sigma$  components will tend to be much more intense than  $\pi$  components.

## 5. Discussion

For the MHD anisotropy to be effective in altering the optical depths, the turbulent velocities must be significant in comparison with the thermal dispersion of the OH molecular velocities. This minimum requirement is easily consistent with the observational data. The thermal velocity  $v_{th}$  for OH is  $\sim 0.3 \text{ km s}^{-1}$ . In contrast, velocity dispersions of at least a few  $\text{km s}^{-1}$  are typical within the region containing a cluster of maser spots (e.g., Argon, Reid, & Menten 2000). The speed of sound for a gas of mostly molecular hydrogen at 100 K is  $0.6 \text{ km s}^{-1}$ . A second condition — that the magnetic pressure exceed the thermal pressure ( $\beta \lesssim 1$ ) — also seems to be satisfied. The observed magnetic field strengths typically are a few to 10 milligauss. Hence,  $\beta = c_s^2/v_A^2 \simeq 0.1[(N/10^7 \text{ cm}^{-3})(T/100 \text{ K})/(B/4\text{mG})^2]$  where a gas density of  $10^7 \text{ cm}^{-3}$   $\text{H}_2$  molecules is adopted as benchmark density based on calculations for the pumping of the masers (Cesaroni & Walmsley 1991; Pavlakis & Kylafis 1996). Although there are uncertainties in the number density  $N$  and the kinetic temperature  $T$ , as well as in the precise maximum value of  $\beta$  that is allowed, it is reasonable to expect from the observations of  $B$  that  $v_A/c_s \gtrsim 3$  for which our calculations in Figure 1 indicate that the magnetic field will be strong enough to create the necessary anisotropy. More generally, equipartition of energy between the turbulent magnetic field and the turbulent motions is suggested both by observations of the interstellar medium and by MHD simulations. Then, even in the absence of a significant uniform magnetic field, the turbulent magnetic field satisfies  $B/(4\pi\rho)^{1/2} \simeq v_t$ , which is equivalent to the statement  $\beta \lesssim 1$  and that  $V_A > c_s$  if the turbulent motions are supersonic.

In addition to (1) the ratio of the turbulent to the OH molecular velocity and (2) the ratio of the thermal to the magnetic pressure ( $\beta$ ), another key consideration is the largest scale length (or minimum wavenumber) at which the turbulence is introduced into the medium



— the outer scale length. Since this determines the maximum length for an elongated masing volume, injection of the turbulence at the largest scale lengths is most effective for creating anisotropy in the optical depths. As noted in §3, a minimum wavenumber  $k_{\min}$  that corresponds to the maximum wavelength  $L/2$  is used for the calculations here. The relationship between the length  $L$  of the edge of the cubic volume within which the fields are computed and actual distances within interstellar clouds can be estimated from the size of a masing spot. In the maps that we compute such as Figure 3, the spectra and intensities change significantly over distances of only a few grid points. We naturally associate this dimension with the “spot size”  $\sim 10^{14}$  cm for mainline OH masers so that the 128 grid points along the edge of a cube correspond to  $L \sim 10^{16}$  cm. This  $L$  is closer to the dimensions of one of the dozen or so clusters of masers in a masing cloud (e.g., Garcia-Barreto et al. 1988) than to the entire cloud. A few computations with  $v_A/c_s = 10$  were performed where the maximum wavelength for injecting the turbulence was reduced to  $L/5$ . The differences between the mean optical depths parallel and perpendicular to the magnetic field analogous to those in Figure 1 are reduced, though the parallel optical depths can still be the larger by about 50% —sufficient for the maser emission along the magnetic field to be more intense by a factor of 100 or more than that perpendicular to  $B$ .

The premise of our calculations that the OH 1665/1667 GHz masers are not highly saturated is supported by the observation that the spectral line breadths tend to be narrower than the thermal breadths for the kinetic temperatures that are expected in the masing gas. The masers may still be somewhat saturated ( $R > \Gamma$ ) as long as the rate  $\gamma$  for velocity/cross relaxation satisfies  $\gamma > R$ .

The OH masers in interstellar clouds are believed to arise in gas that has been influenced by shock waves. Hence, our use of decaying turbulence (as opposed to continuously driven turbulence) seems most appropriate.

Dissipative processes will tend to erase structure in the gas at small scales. We need to check that the dissipation scale is smaller than our numerical resolution in the simulations and smaller than the maser spots  $\sim 10^{14}$  cm. For  $N \sim 10^7 \text{ cm}^{-3}$ ,  $T \sim 10^2 \text{ K}$ , and a fractional ionization  $x \sim 10^{-6}$ , the dominant dissipative process will be ambipolar diffusion. In linear theory, ambipolar diffusion critically damps an Alfvén wave when the wave frequency  $kv_A$  (calculated in the absence of ambipolar diffusion) is comparable with the collision frequency  $\nu_{nI} \approx xN\langle\sigma v\rangle_{In}$  between a neutral and an ion, where  $\langle\sigma v\rangle_{In} = 1.9 \times 10^{-9} \text{ cm}^3 \text{ s}^{-1}$  (Kulsrud & Pearce 1969). This corresponds to  $\lambda_D \sim 10^{13}(T/100 \text{ K})^{1/2}\beta^{-1/2}(10^7 \text{ cm}^{-3}/N)(10^{-6}/x)$ , or somewhat less than the size of a maser spot.

The MHD anisotropy for optical depths parallel and perpendicular to the magnetic field also applies to other spectral lines—both masing and non-masing (or “thermal”) spectral

lines. These differences in the optical depths may lead to anisotropic (or “ $m$ -dependent”) pumping as has been considered previously for the linear polarization of both masing (Western & Watson 1983, 1984) and thermal (Goldreich & Kylafis 1981, 1982; Deguchi & Watson 1984; Lis et al. 1988) spectral lines where the Zeeman splitting is much less than the spectral linebreadth. When applied to the pumping of OH masers, this anisotropy may also contribute significantly to the polarization of OH masers and to the suppression of the  $\pi$  component.

In contrast to our idealized calculation with phenomenological pumping rates and only two energy levels, Gray & Field (1995) calculated the excitation and transport of polarized OH maser radiation in a magnetic field including explicitly the magnetic substates of a number of the energy levels of the OH molecule. The important idea that  $\sigma$  radiation would be strongly beamed in the direction parallel to the magnetic field and  $\pi$  radiation beamed perpendicular to the magnetic field was recognized there. However, at that time no cause was recognized for suppressing the propagation of maser radiation perpendicular to the magnetic field in comparison with that parallel to the magnetic field, and hence for ultimately suppressing the  $\pi$  components in comparison with the  $\sigma$  components.

Faraday rotation within a source tends to destroy the linear polarization of radiation and has sometimes been mentioned as a possible cause for the absence of the linearly polarized  $\pi$  components and for the general tendency for circular polarization to dominate in OH masers. For unsaturated masing and large Faraday rotation, equations (10) and (11) would become (GKK, eq. 56 & 57)

$$I_{\pm} = (I_c/2) \exp[\tau_0(1 + |\cos \theta|)^2/4] \quad (25)$$

and

$$I_0 = (I_c/2) \exp[\tau_0 \sin^2 \theta/2] \quad (26)$$

The modification is thus equivalent to reducing the magnitude of the optical depth of the  $\pi$  component by a factor of two at all angles while leaving the intensity of the  $\sigma$  components essentially unchanged at angles near  $\theta = 0$  where they are most intense. Its effect on the relative intensities of the  $\pi$  and  $\sigma$  components could be at least as great as what we have calculated for the influence of MHD turbulence. Faraday rotation depends on the column density of free electrons through the masing region and on the component of the magnetic field parallel to the line of sight (e.g., Spitzer 1978, pg. 66). While an adequate estimate of the latter can be obtained from the observations, the column density of free electron is highly uncertain and reasonable estimates seem to allow the possibility that Faraday rotation could be either large or negligible for the 1665/1667 MHz OH masers. However, a compelling argument against Faraday rotation as the general cause for the absence of the  $\pi$  components is the observation that, although circular polarization dominates, linearly polar-

ized radiation frequently is detected in the  $\sigma$  components. If Faraday rotation were always strong enough to suppress the  $\pi$  components, it would also be strong enough to eliminate completely the linear polarization of the  $\sigma$  components—in conflict with the observations. Again, considering Faraday rotation in the regime of saturated masing does not help. In the limit of large Faraday rotation and high saturation, the  $\sigma$  components must be completely circularly polarized and, in principle, the three intensities  $I_{\pm}$  and  $I_0$  are equal at all angles (GKK, eq. 47).

Although fractional linear polarizations of 10% or so are probably compatible with our calculations as they stand for suppressing the  $\pi$  components, higher linear polarizations ( $\gtrsim 30\%$ ) are detected in some clouds in a small fraction of the components and these are interpreted as  $\sigma$  components (e.g., Garcia-Barreto et al. 1988; Gasiprong, Cohen, & Hutawarakorn 2002; Slysh et al. 2002). Note that circular polarization in a feature may not assure that the feature is a  $\sigma$  component since a fraction of the linear polarization can, in principle, be converted into circular polarization by Faraday rotation or magnetorotation. If these are in fact  $\sigma$  components, they present a challenge. This radiation must, presumably, be emitted at large angles  $\theta$  relative to the magnetic field as seen from equation (13) and Figure 2. At these large angles, the optical depths of the  $\pi$  components would be expected to be comparable to the optical depths of the  $\sigma$  components and hence to be detected in similar (albeit small) numbers—in apparent conflict with the observations. However, we reason that there are additional considerations which may still allow the suppression of the  $\pi$  components to be understood within the context of the anisotropy of MHD turbulence. (1) Our simplifications in considering only two energy levels and in ignoring any interaction between beams of maser radiation propagating in different directions may be inadequate. When these effects are included, Gray and Field (1995) find that the  $\pi$  components are further suppressed if the optical depths favor directions along the field lines. (2) The anisotropy noted above in the optical depths of the radiation involved in the pumping will tend to cause the populations of the magnetic substates to be unequal, and also potentially contribute to suppressing the  $\pi$  components. Despite this deficiency in the present calculations, it seems clear that MHD turbulence can create an anisotropic environment in interstellar clouds, and that the  $\pi$  components will tend to be suppressed while the circular polarization is favored in the spectra of the mainline OH masers in this environment.

This work was supported in part by a NASA GSRP Fellowship Grant S01-GSRP-044 to JCM, an NCSA Faculty Fellowship for CFG, and NSF Grants AST-9988104 and AST-0093091, and NASA grant NAG 5-9180. Some of our computations were done on NCSA’s platinum cluster. We are grateful to H. W. Wyld for helpful discussions.

## REFERENCES

- Anderson, N. & Watson, W. D. 1993, *ApJ*, 407, 620
- Argon, A. L., Reid, M. J., & Menten, K. M. 2000, *ApJS*, 129, 159
- Armstrong, J. W., Rickett, B. J., & Spangler, S. R. 1995, *ApJ*, 443, 209
- Baudry, A., Desmurs, J.F., Wilson, T.L., & Cohen, R.J. 1997, *A&A*, 325, 255
- Baudry, A., & Diamond, P.J. 1998, *A&A*, 331, 697
- Cesaroni, R., & Walmsley, C.M. 1991, *A&A*, 241, 537
- Caswell, J.L., & Vaile, R.A. 1995, *MNRAS*, 273, 328
- Chandrasekhar, S. 1960, *Radiative Transfer* (New York: Dover)
- Cook, A.H. 1966, *Nature*, 211, 503
- Cho, J. & Vishniac, E. T. 2000, *ApJ*, 539, 273
- Cho, J., Lazarian, A., & Vishniac, E. T. 2002, *ApJ*, 564, 291
- Cho, J. & Lazarian, A. 2003, *Revista Mexicana de Astronomia y Astrofisica Conference Series*, 15, 293
- Condon, E.U., & Shortley, G.H. 1970, *The Theory of Atomic Spectra* (Cambridge: Cambridge U. Press)
- Deguchi, S., & Watson, W. D. 1984, *ApJ*, 285, 126
- Deguchi, S., & Watson, W. D. 1986, *ApJ*, 300, L15
- Evans, C. R. & Hawley, J. F. 1988, *ApJ*, 332, 659
- Garcia-Barreto, J. A., Burke, B. F., Reid, M. J., Moran, J. M., Haschick, A. D., & Schilizzi, R. T. 1988, *ApJ*, 326, 954
- Gasprong, N., Cohen, R. J., & Hutawarakorn, B. 2002, *MNRAS*, 336, 47
- Goldreich, P., Keeley, D. A., & Kwan, J. Y. 1973a, *ApJ*, 179, 111 [GKK]
- Goldreich, P., Keeley, D. A., & Kwan, J. Y. 1973b, *ApJ*, 182, 55
- Goldreich, P., & Kylafis, N. 1981, *ApJ*, 243, L75

- Goldreich, P., & Kylafis, N. 1982, *ApJ*, 253, 606
- Goldreich, P. & Sridhar, S. 1995, *ApJ*, 438, 763
- Gray, M. D. & Field, D. 1995, *A&A*, 298, 243
- Higdon, J. C. 1984, *ApJ*, 285, 109
- Hutawarakorn, B., Cohen, R. J., & Brebner, G. C. 2002, *MNRAS*, 330, 349
- Kulsrud, R., & Pearce, W. P. 1969, *ApJ*, 156, 445
- Lis, D. C., Goldsmith, P. F., Dickman, R. L., Predmore, C. R., Omont, A., & Cernicharo, J. 1988, *A&A*, 328, 304
- Lithwick, Y. & Goldreich, P. 2001, *ApJ*, 562, 279
- Maron, J. & Goldreich, P. 2001, *ApJ*, 554, 1175
- Montgomery, D. & Turner, L. 1981, *Physics of Fluids*, 24, 825
- Moran, J.M., Reid, M.J., Lada, C.J., Yen, J.L., Johnston, K.J., and Spencer, J.H. 1978, *ApJ*, 224, L67
- Narayan, R., Anantharamaiah, K. R., & Cornwell, T. J. 1989, *MNRAS*, 241, 403
- Nedoluha, G.E., & Watson, W.D. 1990, *ApJ*, 361, 653
- Pavlaklis, K.G., & Kylafis, N.D. 1996, *ApJ*, 467, 300
- Reid, M.J. 2002, in *Cosmic Masers: From Protostars to Blackholes*, IAU Symposium 206 (San Fransisco: ASP)
- Slysh, V. I., Mignes, V., Val'tts, I., E., Lyubchenko, S., Yu., Horiuchi, S., Altunin, V., I., Fomalont, E., B., & Inoue, M. 2002, *ApJ*, 564, 317
- Spitzer, L. 1978, *Physical Processes in the Interstellar Medium* (New York: Wiley)
- Stone, J. M., Ostriker, E. C., & Gammie, C. F. 1998, *ApJ*, 508, L99
- Stone, J. M. & Norman, M. L. 1992, *ApJS*, 80, 791
- Vestuto, J. G., Ostriker, E. C., & Stone, J. M. 2003, *ApJ*, 590, 858
- Watson, W. D. & Wyld, H. W. 2001, *ApJ*, 558, L55

Watson, W. D. & Wyld, H. W. 2003, ApJ, 598, 357

Western, L.R., & Watson, W. D. 1983, ApJ, 275, 195

Western, L.R., & Watson, W. D. 1984, ApJ, 285, 158

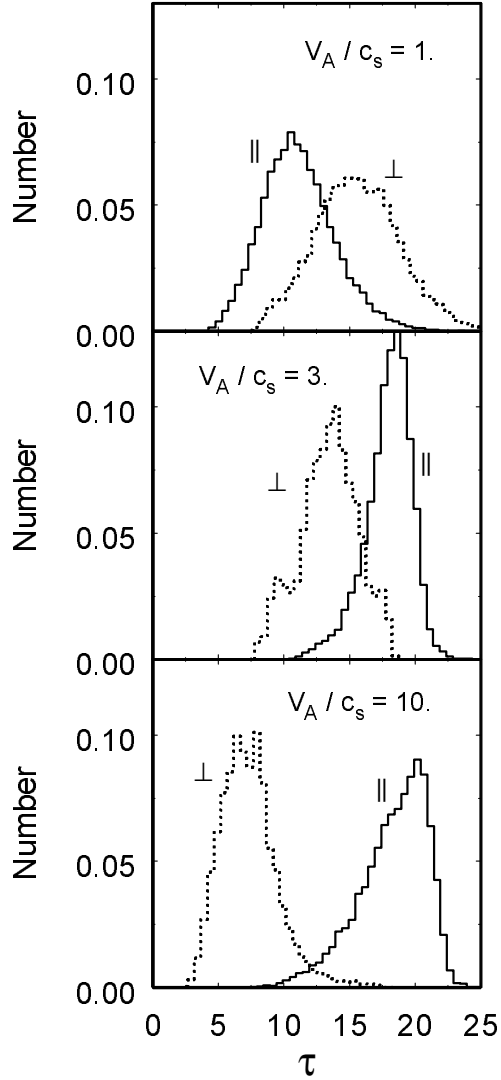


Fig. 1.— Representative histograms for the number of rays with unsaturated optical depths  $\tau$ . The optical depth is obtained at the peak intensity of each ray. The numbers are given as a fractions of the  $128^2$  rays from the surface of a turbulent cube within intervals of 0.5 in  $\tau$ . Separate histograms (as indicated) are shown for rays that propagate parallel and perpendicular to the average magnetic field of the turbulent cube for the three choices  $v_A/c_s = 1, 3,$  and  $10$ .

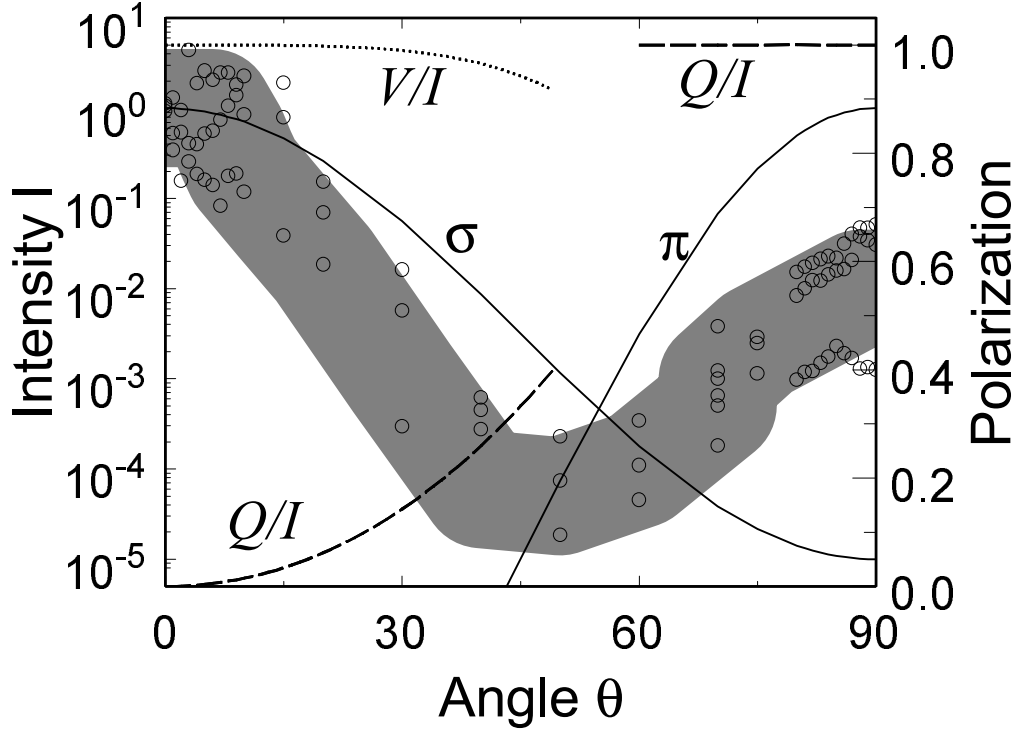


Fig. 2.— The intensity  $I$  (indicated by open circles and in units of the saturation intensity  $I_s$ ) for the brightest maser ray that emerges from a turbulent cube is plotted for several representative cubes with  $v_A/c_s = 3$  as a function of the angle between the ray and the magnetic field, and with the constant for the pumping chosen so that  $I = 1$  at  $0^\circ$  for each cube. The intensities that individual  $\sigma$  and  $\pi$  components would have for unsaturated masing in a uniform medium are plotted (solid lines) for comparison (equations 10 and 11). At angles less than  $55^\circ$ , the fractional circular ( $V/I$ ) and linear ( $Q/I$ ) polarizations are plotted for this unsaturated  $\sigma$  component (equations 12 and 13); for angles greater than  $55^\circ$ , the fractional linear polarization is plotted for the  $\pi$  component (equation 15). The polarizations of the intensities of all rays at a particular angle that are computed using the turbulent cubes and for which the intensities are within 3% of the brightest ray at that angle have polarizations that are essentially identical with those of the unsaturated  $\sigma$  and  $\pi$  components in a uniform medium. The fractional circular and linear polarizations of the unsaturated components in a uniform medium are indicated by dashed and dotted lines, respectively.



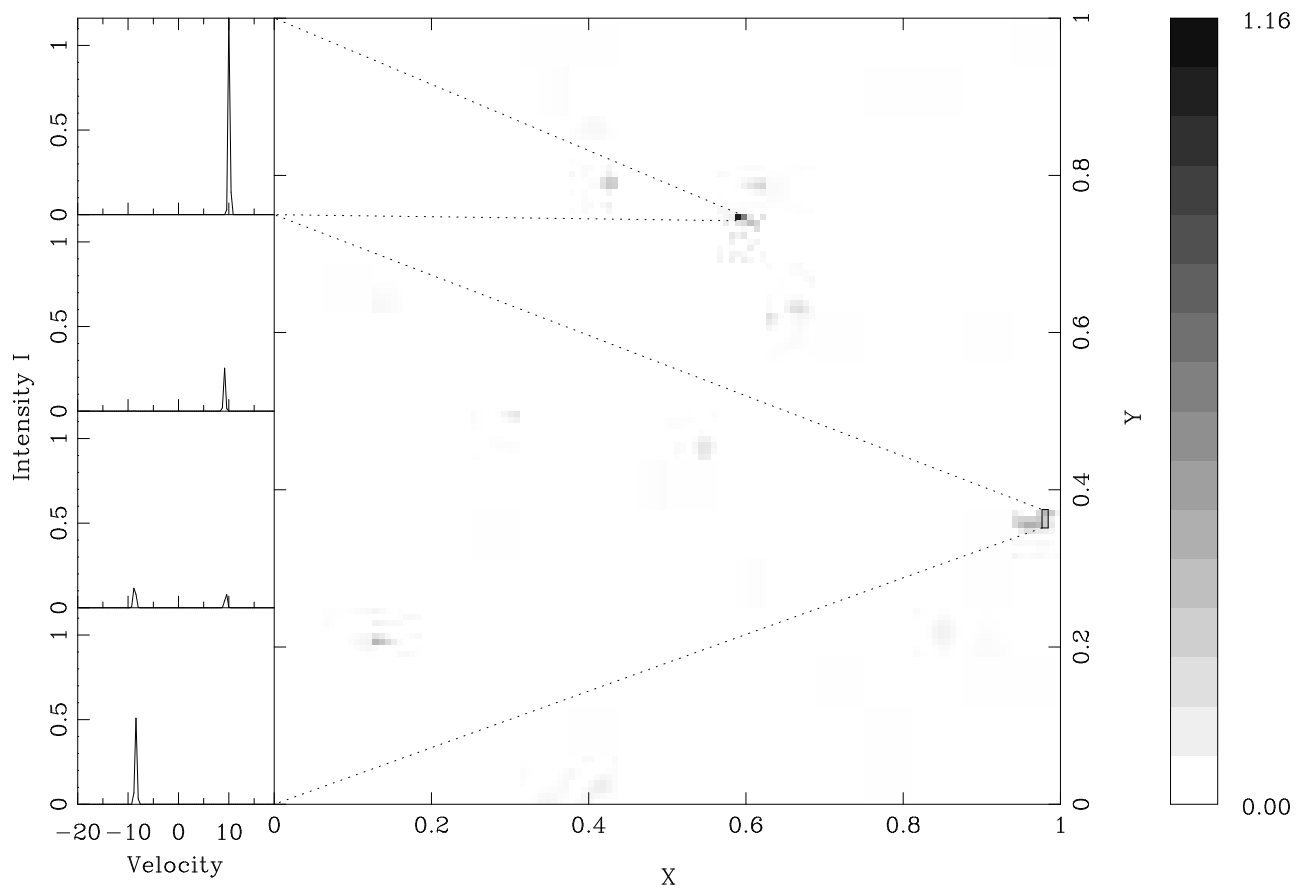


Fig. 3.— Representative grayscale map of the intensities  $I$  (in units of  $I_s$ ) that emerge from the face of a turbulent cube with  $v_A/c_s = 3$  and parallel to the direction of the magnetic field. The panels on the left show the spectra for the rays taken from selected locations on the map as indicated. The Doppler velocity scale is in thermal breadths  $v_{th}$  for the OH molecule.

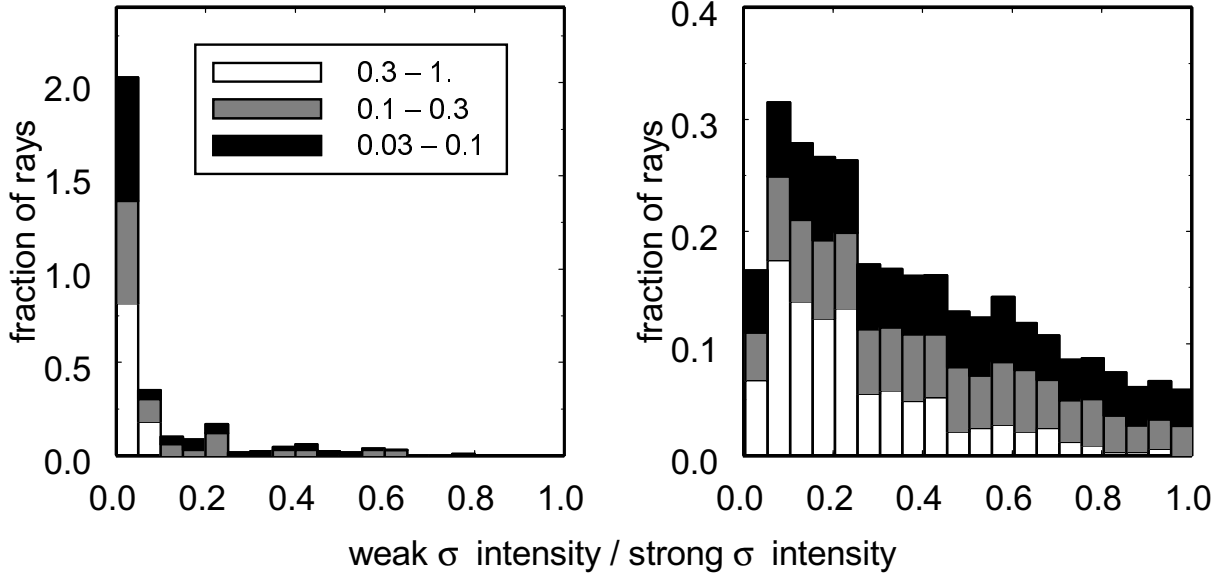


Fig. 4.— Examples of the ratio of the weaker to the stronger of the  $\sigma$  components of the Zeeman pairs for turbulent cubes with  $v_A/c_s = 3$ . The lefthand histogram is computed for the turbulent cube in Figure 2. Only the rays with intensities greater than 0.03 of the brightest ray are included. The rays are grouped as fractions of the intensity of the brightest ray. Those with intensities from 0.03 to 0.1 of the brightest ray are indicated by black; those with intensities between 0.1 and 0.3 of the brightest, by gray; those with intensities between 0.3 and the brightest, by white. The scale for each of these groups is normalized so that for each group, the sum in all columns of a type is one (and the sum of all columns is three). The bins are 0.05 in width. For some 75% of all rays in the lefthand histogram, the ratio is less than 0.05. The righthand histogram is an example where there are more Zeeman pairs.